Ultrathin In_2O_3 Nanowires with Diameters below 4 nm: Synthesis, Reversible Wettability Switching Behavior, and Transparent Thin-Film Transistor Applications

Guozhen Shen,[†,*] Bo Liang,[†] Xianfu Wang,[†] Hongtao Huang,[†] Di Chen,[†] and Zhong Lin Wang[†,‡,*]

[†]Wuhan National Laboratory for Optoelectronics and College of Optoelectronic Science and Engineering, Huazhong University of Science and Technology, Wuhan 430074, China, and [‡]School of Materials Science and Engineering, Georgia Institute of Technology, Atlanta, Georgia 30332-0245, United States

ABSTRACT Ultrafine one-dimensional (1-D) semiconducting nanostructures with diameters below 10 nm are attracting great research attention. Using a laser-ablation chemical vapor deposition (CVD) method, we reported the synthesis of single-crystal In_2O_3 nanowires with diameter below 4 nm. The as-synthesized ultrathin In_2O_3 nanowires act as the ultrathin branches of hierarchical In_2O_3 nanostructures and show fast photoinduced switching surface wettability behaviors, and the contact angle decreased from 134.3 to 0° in 10 min. Transparent thin-film transistors (TTFTs) were fabricated using the as-synthesized product, and the device conductance was 1−2 orders higher than the average conductance of the In_2O_3 single nanowire devices, revealing good opportunity in transparent electronics.

KEYWORDS: In_2O_3 · nanowires · ultrathin · transparent · transistors

In recent years, great attention has been paid to ultrathin one-dimensional (1-D) nanostructures with diameters less than 10 nm. One feature of ultrathin 1-D nanostructures is the significant increased surface area, which in turn has great influence on the performance of chemical/biosensors and catalysts. Besides, due to the ultrathin diameters, ultrathin 1-D nanostructures also showed controlled surface charge, controlled wettability, and quantum conductance and ballistic conduction.[1−18] Many methods have been developed to synthesize 1-D nanostructures, among which the solution methods are the most commonly used ones, which can be found in a recently published review paper by Ozin *et al.*[19] Many kinds of ultrathin 1-D nanostructures, including metals, II−V and III−V group semiconductors, *etc.*, have been produced until now. For example, Hyeon *et al.* reported the synthesis of single unit cell thick samaria nanowires and quantum well structured CdSe nanoribbons.[13] Liu *et al.* produced ultrathin single-crystal ZnS nanowires with diameters down to 1.2 nm.[16] Wang *et al.* synthesized ultrathin single-crystal ZnS nanowires with an average diameter of 4.4 nm.[17] Wang *et al.* synthesized ultrathin InOOH nanowires with a diameter of about 2 nm and lengths up to 200 nm.[18] Murray *et al.* synthesized ultrathin PbSe nanowires with diameters around 5 nm.[20] Ultrathin Au nanowires formed by the oriented attachment reaction were reported by several groups.[21,22] Very recently, the high-temperature vapor phase methods were also developed to synthesize ultrathin 1-D nanostructures, which were able to produce ultrathin nanostructures with better crystallinity and electronic properties.[23,24] For example, Lieber *et al.* reported the synthesis of molecular-scale silicon nanowires using the gold nanocluster-catalyzed vapor method.[24] We previously reported the synthesis of ultrathin ZnO nanowires with diameters of around 6 nm.[4]

Indium oxide (In_2O_3) is a wide band gap transparent semiconductor with a direct band gap around 3.6 eV and an indirect band gap around 2.5 eV.[25−27] It has been widely used in electronic, optoelectronic devices, such as transparent electronics, flat panel displays, light-emitting diodes, solar cells, and gas sensors. Over the past years, several techniques have been developed to synthesize 1-D In_2O_3 nanostructures including nanowires, nanotubes, and nanobelts.[28−40] For instance, Ren *et al.* synthesized In_2O_3 nanowire networks *via* a vapor transport and condensation process.[29] Liang *et al.* synthesized In_2O_3 nanofibers with rectangular cross sections *via* a rapid heating process.[30] Zhou

* Address correspondence to gzshen@mail.hust.edu.cn, zhong.wang@mse.gatech.edu.

Received for review February 17, 2011 and accepted July 12, 2011.

Published online July 12, 2011
10.1021/nn2014722

et al. synthesized diameter-controlled In_2O_3 nanowires *via* a laser-ablation chemical vapor deposition method.[31] Yang *et al.* synthesized porous In_2O_3 nanotubes *via* a layer-by-layer assembly on carbon nanotube templates technique.[33] Chern *et al.* reported the synthesis of vertical In_2O_3 nanowires *via* an epitaxial growth process.[34] Meyyappan *et al.* produced In_2O_3 nanowires on a sapphire substrate.[35] However, all of these reported 1-D In_2O_3 nanostructures have diameters beyond 10 nm, and to the best of our knowledge, there is no report about ultrathin In_2O_3 nanowires with diameters less than 5 nm.

In this work, using a laser-ablation chemical vapor deposition (CVD) method, we reported the synthesis of single-crystal In_2O_3 nanowires with diameter below 4 nm. The as-synthesized ultrathin In_2O_3 nanowires act as the ultrathin branches of hierarchical In_2O_3 nanostructures. In fact, hierarchical assembly of 1-D nanostructures has become one of the hottest topics, recently, due to the fact that hierarchical nanostructures may offer fundamental scientific opportunities for investigating the influence of size and dimensionality with respect to their collective optical, magnetic, and electronic properties and would provide possibilities to probe brand new properties and applications resulting from the spatial orientation and arrangement of the 1-D building blocks.[41,42] Our studies found that the as-synthesized ultrathin nanostructures show fast photoinduced switching surface wettability. Transparent thin-film transistors (TTFTs) were fabricated using the synthesized product, revealing good opportunity in transparent electronics.

RESULTS AND DISCUSSION

Ultrathin In_2O_3 nanowires were grown on In_2O_3 nanowire backbones, formed into hierarchical In_2O_3 nanostructures, *via* a one-step laser-ablation CVD method using an InAs target. After synthesis, a wax-like layer was found deposited on the silicon substrate. The product was characterized by X-ray diffraction (XRD), and the corresponding pattern is depicted in the inset of Figure 1a. Except the peak marked with # (coming from the silicon substrate), all of the other detectable peaks can be indexed to In_2O_3 with cubic phase (JCPSD Card, No. 65-3170), indicating the formation of pure In_2O_3 product or the concentration of the possible impurity is below the detection limit of the XRD machine.

Figure 1a shows a general scanning electron microscopy (SEM) image of the as-synthesized In_2O_3 nanostructures. One-dimensional nanostructures were found to deposit on a large scale. A higher-magnification SEM image is demonstrated in Figure 1b. The as-synthesized 1-D In_2O_3 nanostructures were found to be of hierarchical backbone branch structures. The backbone nanowires have diameters of around 20 nm and lengths up to several tens of micrometers. Figure 1c is a high-magnification SEM image of the ultrathin In_2O_3 nanowire branches grown on the backbone nanowire, where the ultrathin nanowires were found to have very small diameters, smaller than 5 nm according to the image.

To get more information on the obtained ultrathin nanowires, transmission electron microscopy (TEM) was performed. Figure 2a is a TEM image of the ultrathin In_2O_3 nanowires. From the image, the nanowires were found to have diameters below 4 nm with lengths up to 1 μm, indicating the formation of high aspect ratio ultrathin nanowires. Figure 2b gives a clearer TEM image of several typical as-synthesized ultrathin In_2O_3 nanowires, indicating very small diameters. Tens of as-synthesized nanowires were checked, and the results indicate that more than 90% of the nanowires have diameters below 4 nm (Supporting Information, Figure S1), confirming the formation of ultrathin nanowires. Figure 2c shows the TEM image of the tip parts of several as-synthesized ultrathin nanowires. From the image, we can clearly see that dark nanoparticles were attached to their tips, indicating the possible vapor–liquid–solid growth mechanism.

High-resolution TEM (HRTEM) images of several ultrathin In_2O_3 nanowires are shown in Figure 2d,e. From these images, despite the ultrathin diameters of the as-synthesized nanowires, they also have single-crystalline nature, as illustrated by the well-resolved lattice structure of an individual nanowire. The observed lattice fringes in Figure 3d,e were calculated to be around 0.25 nm, corresponding to the [100] plane of cubic In_2O_3 phase. These results indicate that the preferred growth direction of the ultrathin In_2O_3 nanowires is along the [100] orientation. Figure 2f shows the TEM image of the junction part between the backbone nanowire and an ultrathin nanowire branch. The resolved lattice fringe is calculated to be 0.25 nm for both the backbone nanowire and the nanowire branch, indicating that the growth direction for them is [010] and [100], respectively. No obvious defect was observed from the interface part from the image. To get more clear information about the possible growth mechanism, the composition and microstructures of the nanoparticle and the ultrathin nanowire were investigated in detail by using HRTEM. A higher-magnification TEM image of the attached nanoparticle is depicted in Figure 2g. Energy-dispersive X-ray spectrometry (EDX), detected by nanobeam with a spot size of 20 nm, was used to check the composition of the attached dark nanoparticle and the nanowire, respectively. Figure 2h is the EDX spectra of the nanowire. Besides the peaks of C and Cu (coming from carbon-coated TEM grid), the presence of only In and O indicates the formation of pure In_2O_3 phase. From the spectrum, no peak from As was detected to the

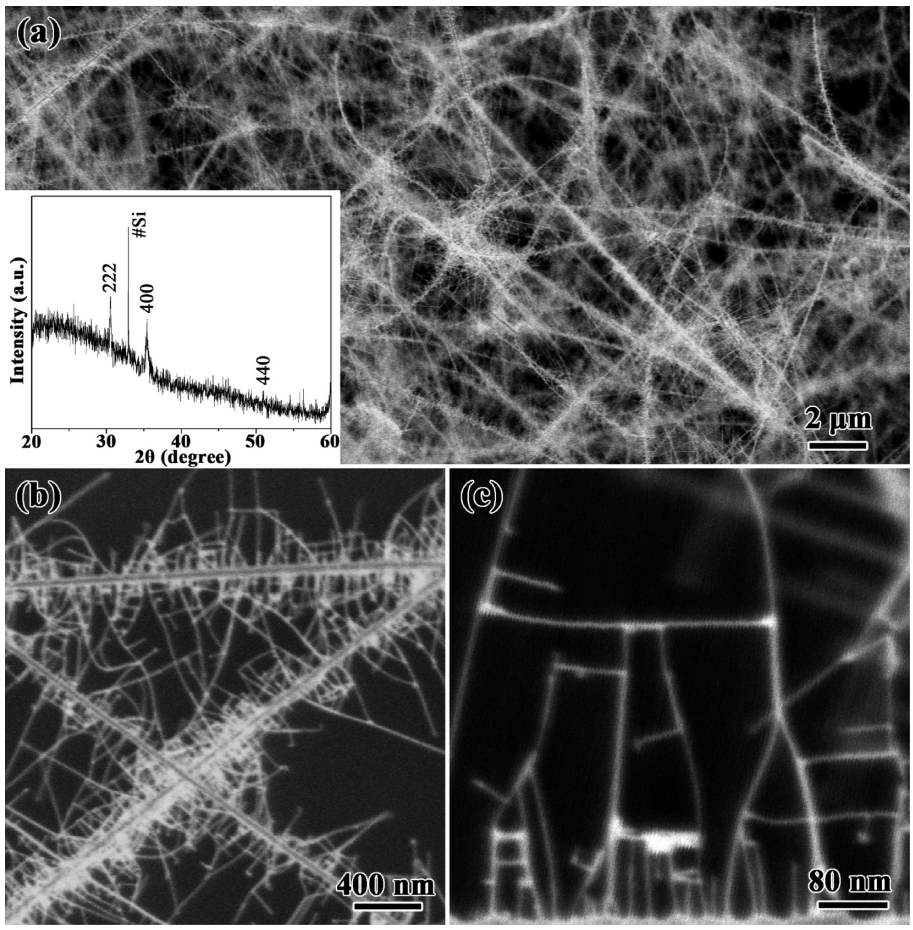

Figure 1. SEM images of the as-synthesized hierarchical In_2O_3 nanostructures, consisting of ultrathin In_2O_3 nanowires as the branches. Inset is an XRD pattern of the product.

limit of our equipment, indicating that either there is no As or the concentration of As is lower than the detection limit of the TEM machine. The EDX spectrum of the attached nanoparticle is shown in Figure 2i, which reveals that the nanoparticle is mainly composed of Au. It confirms that the ultrathin nanowires were governed by the VLS mechanism. The junction part between the Au nanoparticle and the In_2O_3 nanowire was also studied, as depicted in Figure 2j (obtained from the part framed in Figure 2g). The observed lattice fringes from the ultrathin In_2O_3 nanowire and the Au nanoparticle were calculated to be 0.25 and 0.235 nm as marked in the image, corresponding to the [100] plane of cubic In_2O_3 phase and the [111] plane of cubic Au phase, respectively.

Figure 2k is a TEM image of an individual backbone In_2O_3 nanowire, which has a diameter of around 20 nm. Au nanoparticle with a diameter of around 20 nm was also observed to be attached to the backbone nanowire, also indicating that the backbone nanowires were governed by the VLS mechanism. The junction part between the backbone In_2O_3 nanowire and the Au nanoparticle was also studied by using HRTEM, and the result is shown in Figure 2l. The calculated lattice fringes from the backbone In_2O_3 nanowire and the Au nanoparticle were also calculated to be 0.25 and 0.235 nm. Similar to the result from Figure 2g, the lattices correspond to the [100] plane of cubic In_2O_3 phase and the [111] plane of cubic Au phase, respectively.

From the above results, we can see that both the backbone nanowires and the ultrathin nanowires are governed by the VLS mechanism. The whole process can be expressed as follows. During the reaction, InAs was ablated and decomposed to generate In clusters/droplets due to the high energy laser beam. The newly generated In clusters/droplets were then oxidized by the remaining oxygen to form In_2O_3 nanowires catalyzed by 20 nm Au nanoparticles, resulting in the formation of backbone nanowires with diameters of ~20 nm. At the same time, Au nanoparticles were gradually evaporated and generated new Au nanoclusters, which then deposited on the newly formed backbone In_2O_3 nanowires. They acted as the catalysts for the secondary growth of ultrathin In_2O_3 nanowire branches. With prolonged reaction time, the density of the ultrathin nanowires should gradually increase. To confirm the speculation, we checked the intermediate products by collecting the samples at different reaction times. Figure 3a,b shows the SEM results of

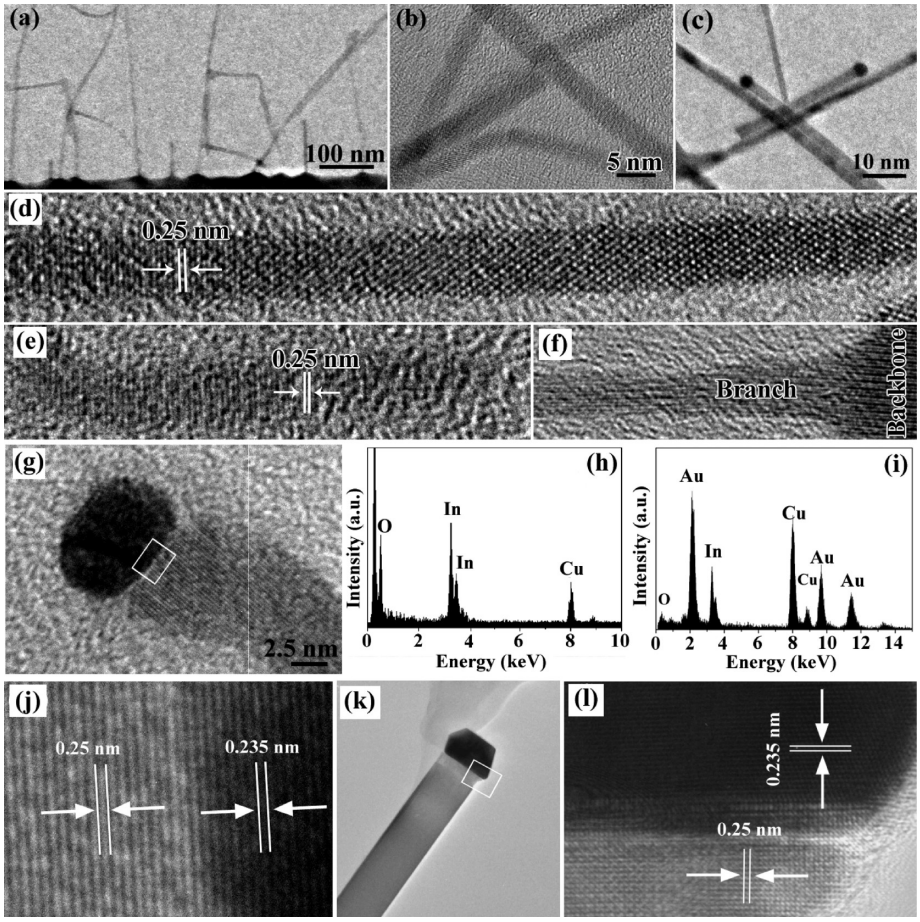

Figure 2. (a) TEM image of the ultrathin In_2O_3 nanowires. (b) TEM image showing the ultrathin diameters of around 4 nm. (c) TEM image of several ultrathin nanowires, showing the attached nanoparticles. (d,e) HRTEM image of individual In_2O_3 nanowires, showing the formation of single-crystal nanowires. (f) HRTEM image showing the junction part between the ultrathin nanowire branch and the nanowire backbone. (g) TEM image of a single nanowire, showing the attached nanoparticle on its tip. (h,i) EDX spectra taken from the nanowire and the attached nanoparticles, revealing the formation of In_2O_3, and the attached nanoparticle is Au. (j) HRTEM image taken from the interface part framed in panel g. (k) TEM image of a backbone In_2O_3 nanowire. (l) HRTEM image taken from the junction part between the backbone In_2O_3 nanowire and the attached Au nanoparticle framed in panel k.

the samples after they were reacted for 25 and 45 min, respectively. It clearly reveals that the density of the branched ultrathin nanowires grown on the nanowire trunks increased with prolonged reaction time, further confirming the gradual deposition of Au nanoparticles on the backbone nanowires as secondary catalysts. On the basis of the above proposed growth mechanism, we extended it to the synthesis of hierarchical In_2O_3 nanostructures in a conventional CVD system without laser ablation. The results are shown in Figure S2 of the Supporting Information. The backbone nanowires were catalyzed by Au particles with large sizes, while the branched nanowires were catalyzed by Au nanoparticles with diameters of around 100 nm.

The surface wetting behavior of nanostructured thin films, especially nanowire films, has attracted great interests in recent years.[43−47] Contact angle (CA) was usually measured to demonstrate whether the solid surface is hydrophobic or hydrophilic. CA is thought to be governed by two factors: the chemical composition and the roughness of the surface. Herein, we also investigated the surface wettability of the as-synthesized ultrathin In_2O_3 nanowires. To exclude the effect of possible contaminations in air, we measured the contact angle in a clean room. Figure 4a shows a water droplet shape on the nanowire films, revealing the CA of 134.3°. The CA is much larger than that of smooth In_2O_3 films with a CA of around 20°.[40] According to previous reports on nanowire films, it is thought that the surface roughness of nanostructures contained enough room to hold air in the troughs between nanowires, thus resulting in the hydrophobic surface properties.[45]

The photon-induced wettability conversion properties of the ultrathin In_2O_3 nanowires were further explored. UV illumination was carried out using a UV lamp with a wavelength of 254 nm. Figure 4 is the photoinduced reversible wettability of the nanowire film. It clearly reveals that, under UV irradiation, the CA of the water droplet gradually decreased from 134.3 to

0° in 10 min. According to previous reports, under UV illumination, the surface roughness of nanoscale materials magnified the superficial acreage of In_2O_3 and increased the chances of generation of electron−hole pairs in the surface. Some of the holes could react with lattice oxygen to form surface oxygen vacancies, which are kinetically more favorable for hydroxyl (−OH) adsorption, thus resulting in the wettability conversion under UV illumination.[43−47] The wettability conversion from hydrophobic to hydrophilic of the present nanowires is much faster than that of aligned In_2O_3 nanowire arrays,[47] which may be related to the ultrathin diameters of the as-synthesized nanowires. After UV exposure, the exposed ultrathin In_2O_3 nanowires were stored in the dark for several hours, and it was found that the wettability returns to hydrophobic again and the cycles can be repeated. Figure S4 (Supporting Information) is the cycle-related wettability changes *via* UV illumination and dark storage, revealing reversible wettability of the present nanowire films. The phenomena can be explained by the replacement of adsorbed hydroxyls by oxygen in air since oxygen adsorption is thermodynamically more stable.[19−21] It makes the surfaces of the In_2O_3 nanowires return to the initial state and the wettability of the films reconverts to hydrophobic.

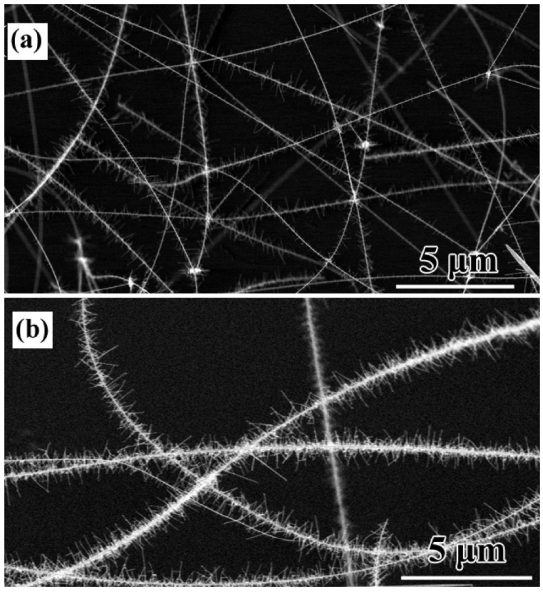

Figure 3. SEM images of the sample after reacting for (a) 25 min and (b) 45 min, respectively.

To get more information about the relationship between the diameters and their corresponding contact angles, we synthesized In_2O_3 nanowires with diameters of 4, 20, 50, and 200 nm. Figure 5 shows the SEM images of In_2O_3 nanowires with different diameters and their corresponding CA values, which are 143° for 4 nm nanowires, 129° for 20 nm nanowires, 88° for 50 nm nanowires, and 61° for 200 nm. The results clearly revealed that the CA decreased with the increase of the diameters of the nanowires. The differences in CA originated from the surface roughness of nanostructure films. In_2O_3 nanowires with smaller diameters contained more room to hold air in the troughs between nanowires, thus resulting in the increase of contact angles. The photon-induced wettability conversion properties of In_2O_3 nanowires with different diameters were also studied, which showed similar trends with the change of CA for different nanostructures. That is to say, the bigger the diameter, the longer the switching between hydrophobic and hydrophilic behaviors. According to the above discussions, we believed that it is related to the change of diameters.

With a wide band gap of around 3.6 eV, In_2O_3 has great applications in transparent electronics because of its high transparency in the visible light region.[25−29] As an example, we demonstrate here the fabrication of transparent thin-film transistors (TTFTs) using the present ultrathin In_2O_3 nanowires grown on backbone nanowires as the active device channel. To make TTFTs, an ITO glass was used as the device substrate, which was sputtered with a thin Al_2O_3 layer with 50 nm thickness by an atomic layer deposition (ALD) method.

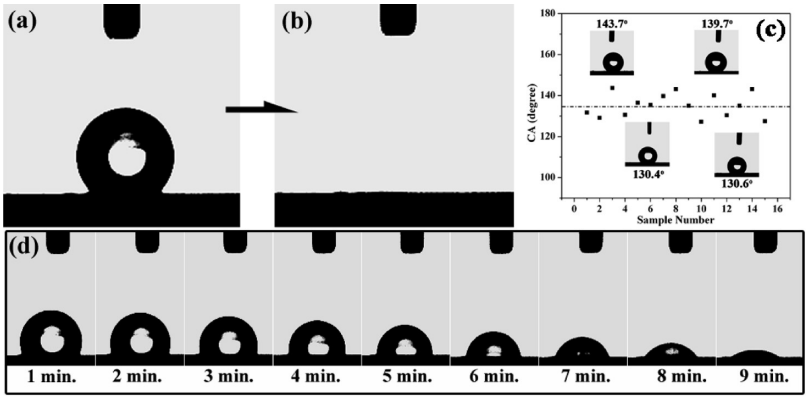

Figure 4. Photoinduced reversible wettability of the In_2O_3 nanostructures. (a) Before and (b) after UV illumination. (c) Contact angles obtained from different samples, showing the hydrophobic properties of the In_2O_3 nanostructures with an average contact angle of about 135°. (d) Optical images showing the gradual decrease of water contact angles under UV illumination.

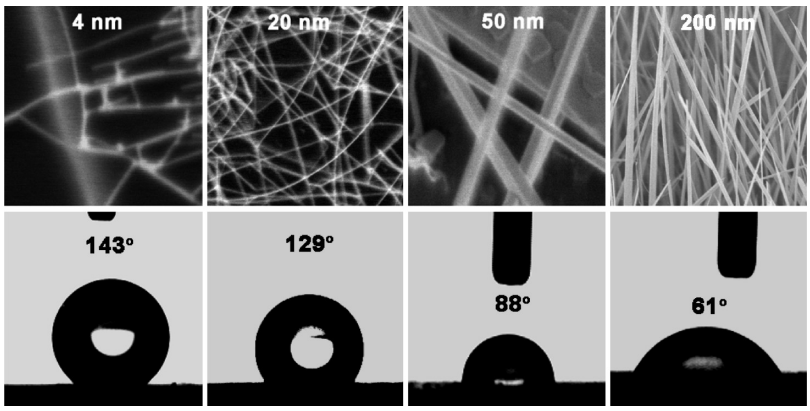

Figure 5. Comparison of contact angles for In_2O_3 nanowires with different diameters.

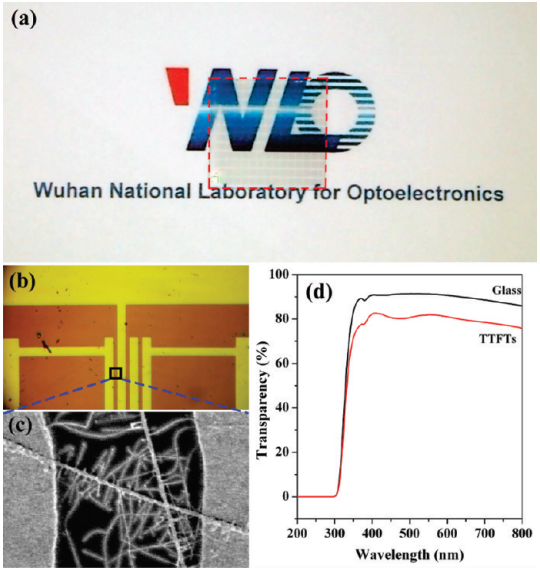

Figure 6. (a) Optical photograph of the fabricated device, showing very good transparency. (b) Optical images show the geometric layout of the transparent TFT devices. (c) SEM image of a device. (d) Optical transmittance of ITO glass substrates and the TTFTs.

The sputtered Al_2O_3 layer acts as the dielectric layer for the transistor. The as-synthesized In_2O_3 nanostructures were ultrasonicated in isopropyl alcohol (IPA) to yield nanowire suspension, which was then dropped onto the ITO glass substrate to form a nanowire thin film. After being dried in vacuum, source and drain electrodes were then patterned on the ITO glass by conventional photolithography, followed by the ion-assisted deposition of ITO. Figure 6a is an optical image of the transparent device. The background photograph is clearly visible through the transistor region, indicating very good transparency. The device structure is depicted in Figure 6b, and a corresponding SEM image of the device is also shown (Figure 6c), where hierarchical nanowires were found gated by two electrodes. Optical transmittance of the TTFTs was also measured, and the data are shown in Figure 6d. It can be seen that as-fabricated TTFTs show ~80% optical transmittance

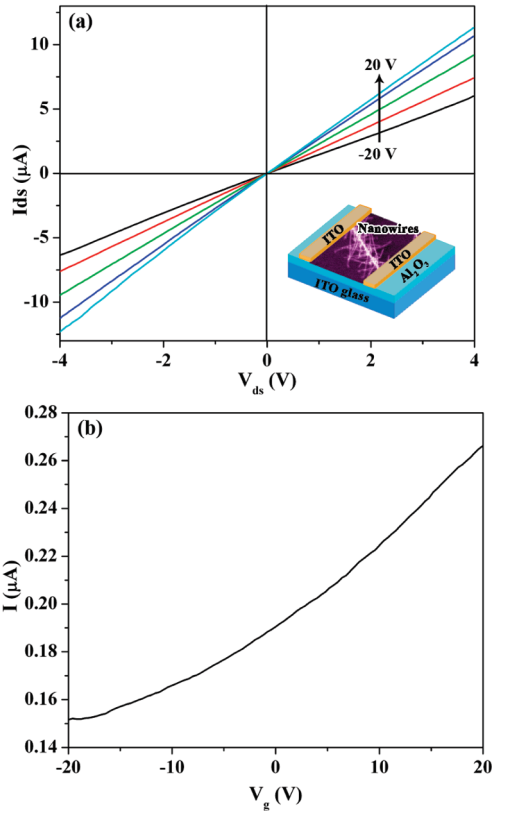

Figure 7. Current–voltage data recorded from a TTFT built on the thin film of hierarchical In_2O_3 nanostructures. The curves correspond to the gate voltage from −20 to 20 V with a step of 10 V. (a) $I_{DS}-V_{DS}$ curves and (b) $I_{DS}-V_G$ transfer curves. Inset is a schematic illustration of the device structure.

in the visible light range, confirming the good transparency.

A schematic illustration of a typical TTFT device is shown in the inset of Figure 7a. The channel width of the device is around 2 μm. The electronic transport behavior of as-fabricated TTFTs was also measured. $I-V$ curves of the device were recorded by sweeping the gate voltage from −20 to 20 V with a step of 10 V, as plotted in Figure 7a. From the data, one can see that with substantially increased current channels, the

transistor showed enhanced conductance, indicating typical n-type semiconducting behavior. The conductance is measured to be about 10.8 μS at V_G = 20 V, 8.4 μS at V_G = 0 V, and 5.9 μS at V_G = −20 V. The values are 1−2 orders higher than the average conductance of the In_2O_3 single nanowire devices,[23] which make the ultrathin In_2O_3 nanowire-based TFTs more suitable for high-performance device applications than single nanowire devices. Compared with a single nanowire device, it was found that the sensitivity to electrostatic gating of the current TTFTs was significantly suppressed. This can be clearly observed in the $I-V_G$ curve shown in Figure 7b, where the maximum transconductance was calculated to be around 0.006 μS and the on/off ratio is around 2. The significantly reduced gating effect might stem from the fact that each TTFT device consisted of a large number of hierarchical In_2O_3 nanowires. Both the backbone nanowires and the ultrathin nanowire branches tend to lay atop each other, which resulted in the fact that the gate dependence is weakened due to the increased average gate−nanowire distance. Similar result was also observed by other researchers when they tried to fabricate multiwire devices.[48,49] We believe that such effect may be applied to make high-performance devices, such as chemical sensors in terms of high stability. In fact, Zhou *et al.* had already demonstrated that multi-nanowire devices with reduced gate effect worked for high-performance chemical sensors, which were able to detect N_2 down to 5 ppb level.[50] Besides, the hierarchical structure of the product made the device fabrication much easier than single nanowires, and the device yield is much better than previously reported single nanowire transistors.[28,50]

In summary, we successfully synthesized ultrathin In_2O_3 nanowires with diameters below 4 nm. As-synthesized ultrathin nanowires were found grown on backbone nanowires *via* a Au migrating catalyzed VLS process. Surface wettability studies showed the hydrophobic behavior with an average CA of about 135°. Besides, the ultrathin nanowires exhibited much faster photoinduced reversible surface wettability from hydrophobic to hydrophilic than their bulk counterpart. Transparent transistors were built on the produced nanostructures, showing a good transparency of around 80% in the visible light region. Due to the hierarchical nature and the ultrathin diameters of the produced samples, the device yield was found to be around 100%. Our results suggest that the current ultrathin In_2O_3 nanowires may find applications in transparent electronics, high-performance chemical sensors, and so on.

EXPERIMENTAL SECTION

Ultrathin In_2O_3 manowires were grown on In_2O_3 nanowire backbones *via* a laser-ablation chemical vapor deposition method. An InAs tablet was used as the ablation target, and Si/SiO_2 wafer was used as the collecting substrate, which was cleaned in acetone and isopropyl alcohol and then coated with Au nanoparticles (20 nm in diameter) serving as the catalysts for the growth of the backbone nanowires. Silicon substrate was loaded into the middle part of a quartz tube of a furnace, and the target was placed at the upper entrance of the furnace. The system was first pumped to eliminate oxygen in the reaction system, and then pure Ar was flown through the system at a rate of 150 sccm. A pulsed Nd:YAG laser with a repetition rate of 10 Hz and a pulse power of 1.0 W was used. During the laser-ablation process, the chamber was maintained at 770 °C under atmospheric pressure, and the reaction time was 45 min. After synthesis, a wax-like layer was found to be deposited on the silicon substrate.

The product was characterized using an X-ray powder diffractometer (RINT 2200), a Hitachi field-emission scanning electron microscope (SEM, S-4800), and a JEOL field-emission transmission electron microscope (TEM, JEM-2010). The surface wettability was investigated by measuring the water contact angle by an SL200B contact angle system (Solon Technology Science Co., Ltd.) at ambient pressure and room temperature. The transparency of the fabricated TTFTs was measured by using a UV/vis spectrometer (UV-2550, Shimadzu). The electronic properties of as-fabricated nanowire TTFTs were examined by using an Agilent 4156 B semiconductor parameter analyzer.

Acknowledgment. This work was supported by National Natural Science Foundation of China (51002059, 21001046), the 973 Projects of China (2011CBA00703), the Natural Science Foundation of Hubei Province (2009CDB326), the Research Fund for the Doctoral Program of Higher Education (20090142120059, 20100142120053), and the Director Fund of WNLO. The authors thank the Analytical and Testing Center of Huazhong University of Science and Technology (HUST) for support.

Supporting Information Available: Diameter distribution of the as-synthesized ultrathin In_2O_3 nanowires, Optical image and SEM images of hierarchical In_2O_3 nanostructures governed by VLS and secondary VLS mechanisms, gradually decreasing of water contact angles under UV illumination, cycle-related wettability changes *via* UV illumination and dark storage. This material is available free of charge *via* the Internet at http://pubs.acs.org.

REFERENCES AND NOTES

1. Xia, Y.; Yang, P.; Sun, Y.; Wu, Y.; Mayers, B.; Gates, B.; Yin, Y.; Kim, F.; Yan, H. One-Dimensional Nanostructures: Synthesis, Characterization, and Applications. *Adv. Mater.* **2003**, *15*, 353–389.
2. Duan, X. F.; Lieber, C. M. Laser-Assisted Catalytic Growth of Single Crystal GaN Nanowires. *J. Am. Chem. Soc.* **2000**, *122*, 188–189.
3. Pan, Z.; Dai, Z.; Wang, Z. L. Nanobelts of Semiconducting Oxides. *Science* **2001**, *291*, 1947–1949.
4. Wang, X. D.; Ding, Y.; Summers, C. J.; Wang, Z. L. Large-Scale Synthesis of Six-Nanometer-Wide ZnO Nanobelts. *J. Phys. Chem. B* **2004**, *108*, 8773–8777.
5. Shen, G. Z.; Chen, D. Self-Coiling $Ag_2V_4O_{11}$ Nanobelts into Perfect Nanorings and Microloops. *J. Am. Chem. Soc.* **2006**, *128*, 11762–11763.
6. Lieber, C. M. Nanoscale Science and Technology: Building a Big Future from Small Things. *MRS Bull.* **2003**, *28*, 486–491.
7. Wang, Z. L. Nanostructures of Zinc Oxide. *Mater. Today* **2004**, *7*, 26–33.

8. Feldman, Y.; Wasserman, E.; Srolovitz, D. J.; Tenne, R. High-Rate, Gas-Phase Growth of MoS_2 Nested Inorganic Fullerenes and Nanotubes. *Science* **1995**, *267*, 222–225.
9. Shen, G. Z.; Chen, D.; Chen, P. C.; Zhou, C. Vapor-Solid Growth of One-Dimensional Layer-Structured Gallium Sulfide Nanostructures. *ACS Nano* **2009**, *3*, 1115–1118.
10. Shen, G. Z.; Bando, Y.; Ye, C.; Yuan, X. L.; Sekiguchi, T.; Golberg, D. Single-Crystalline Nanotubes of II_3-V_2 Semiconductors. *Angew. Chem., Int. Ed.* **2006**, *45*, 7568–7572.
11. Zhang, J.; Chen, P. C.; Shen, G. Z.; He, J. B.; Kumbhar, A.; Zhou, C.; Fang, J. p-Type Field-Effect Transistors of Single-Crystal ZnTe Nanobelts. *Angew. Chem., Int. Ed.* **2008**, *47*, 9469–9471.
12. Patzke, G. R.; Krumeich, F.; Nesper, R. Oxidic Nanotubes and Nanorods: Anisotropic Modules for a Future Nanotechnology. *Angew. Chem., Int. Ed.* **2002**, *41*, 2446–2461.
13. Yu, T.; Joo, J.; Park, Y. I.; Hyeon, T. Single Unit Cell Thick Samaria Nanowires and Nanoplates. *J. Am. Chem. Soc.* **2006**, *128*, 1786–1787.
14. Hoo, J.; Son, J. S.; Kwon, S. G.; Yu, J. H.; Hyeon, T. Low-Temperature Solution-Phase Synthesis of Quantum Well Structured CdSe Nanoribbons. *J. Am. Chem. Soc.* **2006**, *128*, 5632–5633.
15. Ozin, G. A.; Cademartiri, L. Ultrathin Nanowires: A Materials Chemistry Perspective. *Adv. Mater.* **2009**, *21*, 1013–1020.
16. Deng, Z.; Yan, H.; Liu, Y. Controlled Colloidal Growth of Ultrathin Single-Crystal ZnS Nanowires with Magic-Sized Diameter. *Angew. Chem., Int. Ed.* **2010**, *49*, 8695–8698.
17. Zhang, Y.; Xu, H.; Wang, Q. Ultrathin Single Crystal ZnS Nanowires. *Chem. Commun.* **2010**, *46*, 8941–8943.
18. Xu, X.; Wang, X. Size- and Surface-Determined Transformations: From Ultrathin InOOH Nanowires to Uniform c-In_2O_3 Nanocubes and rh-In_2O_3 Nanowires. *Inorg. Chem.* **2009**, *48*, 3890–3895.
19. Cademartiri, L.; Ozin, G. A. Ultrathin Nanowires: A Materials Chemistry Perspective. *Adv. Mater.* **2009**, *21*, 1013–1020.
20. Cho, K. S.; Talapin, D. V.; Gascher, W.; Murray, C. B. Designing PbSe Nanowires and Nanorings through Oriented Attachment of Nanoparticles. *J. Am. Chem. Soc.* **2005**, *127*, 7140–7147.
21. Huo, Z.; Tsung, C. K.; Huang, W.; Zhang, X.; Yang, P. Sub-Two Nanometer Single Crystal Au Nanowires. *Nano Lett.* **2008**, *8*, 2041–2044.
22. Wang, C.; Hou, Y. L.; Kim, J. M.; Sun, S. H. A general Strategy for Synthesizing FePt Nanowires and Nanorods. *Angew. Chem., Int. Ed.* **2007**, *46*, 6333–6335.
23. Xin, G. Z.; Fang, X. S.; Zhang, Z.; Wang, D. D.; Huang, X.; Guo, J.; Liao, L.; Zheng, Z.; Xu, H. R.; Yu, T.; *et al.* Ultrathin Single-Crystal ZnO Nanobelts: Ag-Catalyzed Growth and Field Emission Property. *Nanotechnology* **2010**, *21*, 255701.
24. Wu, Y.; Cui, Y.; Huynh, L.; Barrelet, C. J.; Bell, D. C.; Lieber, C. M. Controlled Growth and Structures of Molecular-Scale Silicon Nanowires. *Nano Lett.* **2004**, *4*, 433–436.
25. Gurlo, A.; Barsan, N.; Ivanovskaya, M.; Weimar, U.; Gopel, W. In_2O_3 and MoO_3-In_2O_3 Thin Film Semiconductor Sensors: Interaction with NO_2 and O_3. *Sens. Actuators, B* **1998**, *47*, 92–99.
26. Shigesato, Y.; Takaki, S.; Haranoh, T. Electrical and Structural Properties of Low Resistivity Thin-Doped Indium Oxide Films. *J. Appl. Phys.* **1992**, *71*, 3356–3364.
27. Liu, Q.; Lu, W.; Ma, A.; Tang, J.; Lin, J.; Fang, J. Study of Quasi-Mondisperse In_2O_3 Nanocrystals: Synthesis and Optical Determination. *J. Am. Chem. Soc.* **2005**, *127*, 5276–5277.
28. Shen, G. Z.; Xu, J.; Wang, X. F.; Huang, H. T.; Chen, D. Growth of Directly Transferable In_2O_3 Nanowire Mats for Transparent Thin-Film Transistor Applications. *Adv. Mater.* **2011**, *23*, 771–775.
29. Lao, J.; Huang, J.; Wang, D. Z.; Ren, Z. F. Self-Assembled In_2O_3 Nanocrystal Chains and Nanowire Networks. *Adv. Mater.* **2004**, *16*, 65–69.
30. Liang, C.; Meng, G. W.; Lei, Y.; Phillipp, F.; Zhang, L. D. Catalytic Growth of Semiconducting In_2O_3 Nanofibers. *Adv. Mater.* **2001**, *13*, 1330–1333.
31. Li, C.; Zhang, D.; Han, S.; Liu, X.; Tang, T.; Zhou, C. Diameter-Controlled Growth of Single-Crystalline In_2O_3 Nanowires and Their Electronic Properties. *Adv. Mater.* **2003**, *15*, 143–146.
32. Shen, G. Z.; Chen, D. Fast-Heating-Vapor-Trapping Method to Aligned Indium Oxide Bi-crystalline Nanobelts Arrays and Their Electronic Properties. *J. Mater. Chem.* **2010**, *20*, 10888–10893.
33. Du, N.; Zhang, H.; Chen, B.; Ma, X.; Liu, Z.; Wu, J.; Yang, D. Porous Indium Oxide Nanotubes: Layer-by-Layer Assembly on Carbon Nanotube Templates and Application for Room-Temperature NH_3 Gas Sensors. *Adv. Mater.* **2007**, *19*, 1641–1645.
34. Chen, C. J.; Xu, W. L.; Chern, M. Y. Low-Temperature Epitaxial Growth of Vertical In_2O_3 Nanowires on a-Plane Sapphire with Hexagonal Cross-Section. *Adv. Mater.* **2007**, *19*, 3012–3015.
35. Nguyen, P.; Ng, H. T.; Yamada, T.; Smith, M. K.; Li, J.; Han, J.; Meyyappan, M. Direct Integration of Metal Oxide Nanowire in Vertical Field-Effect Transistor. *Nano Lett.* **2004**, *4*, 651–657.
36. Kong, X. Y.; Wang, Z. L. Structures of Indium Oxide Nanobelts. *Solid State Commun.* **2003**, *128*, 1–4.
37. Caruntu, D.; Yao, K.; Zhang, Z.; Austin, T.; Zhou, W.; O'Connor, C. J. One-Step Synthesis of Nearly Monodisperse, Variable-Shaped In_2O_3 Nanocrystals in Long Chain Alcohol Solutions. *J. Phys. Chem. C* **2010**, *114*, 4875–4886.
38. Wei, Z. P.; Guo, D. L.; Liu, B.; Chen, R.; Wong, L. M.; Yang, W. F.; Wang, S. J.; Sun, H. D.; Wu, T. Ultraviolet Light Emission and Excitonic Fine Structures in Ultrathin Single-Crystalline Indium Oxide Nanowires. *Appl. Phys. Lett.* **2010**, *96*, 031902.
39. Chen, C.; Chen, D. R.; Jiao, X. L.; Wang, C. Ultrathin Corundum-Type In_2O_3 Nanotubes Derived from Orthorhombic InOOH: Synthesis and Formation Mechanism. *Chem. Commun.* **2006**, 4632–4634.
40. Wang, G.; Park, J.; Wexler, D.; Park, M. S.; Ahn, J. H. Synthesis, Characterization, and Optical Properties of In_2O_3 Semiconductor Nanowires. *Inorg. Chem.* **2007**, *46*, 4778–4780.
41. Manna, L.; Scher, E. C.; Alivisatos, A. P. Synthesis of Soluble and Processable Roa-, Arrow-, Teardrop-, and Tetrapod-Shaped CdSe Nanocrystals. *J. Am. Chem. Soc.* **2000**, *122*, 12700–12706.
42. Gudiksen, M. S.; Lauhon, L. J.; Wang, L.; Smith, D. C.; Lieber, C. M. Growth of Nanowire Superlattice Structures for Nanoscale Photonics and Electronics. *Nature* **2002**, *415*, 617–620.
43. Zhu, W. Q.; Feng, X.; Feng, J.; L. Jiang, L. UV-Manipulated Wettability between Superhydrophobicity and Superhydrophilicity on a Transparent and Conductive SnO_2 Nanorod Film. *Chem. Commun.* **2006**, 2753–2755.
44. Miyauchi, M.; Nakajima, A.; Watanabe, T.; Hashimoto, K. Photocatalysis and Photoinduced Hydrophilicity of Various Metal Oxide Thin Films. *Chem. Mater.* **2002**, *14*, 2812–2816.
45. Chen, A. C.; Peng, X. S.; Koczkur, K.; Miller, B. Super-Hydrophobic Tin Oxide Nanoflowers. *Chem. Commun.* **2004**, 1964–1965.
46. Yan, B.; Tao, J.; Pang, C.; Zheng, Z.; Shen, Z.; Alfred, C.; Huan, H.; Yu, T. Reversible UV-Light-Induced Ultrahydrophobic-to-Ultrahydrophilic Transition in an α-Fe_2O_3 Nanoflakes Film. *Langmuir* **2008**, *24*, 10569–10571.
47. Zhong, M.; Zheng, M.; Zeng, A.; Ma, L. Direct Integration of Vertical In_2O_3 Nanowire Arrays, Nanosheet Chains, and Photoinduced Reversible Switching of Wettability. *Appl. Phys. Lett.* **2008**, *92*, 093118.
48. Zhang, D.; Liu, Z.; Li, C.; Tang, T.; Liu, X.; Han, S.; Lei, B.; Zhou, C. Detection of NO_2 Down to ppb Levels Using Individual and Multiple In_2O_3 Nanowire Devices. *Nano Lett.* **2004**, *4*, 1919–1924.
49. Dattoli, E. N.; Wan, Q.; Guo, W.; Chen, Y.; Pan, X.; Lu, W. Fully Transparent Thin-Film Transistor Devices Based on SnO_2 Nanowires. *Nano Lett.* **2007**, *7*, 2463–2469.
50. Chen, P. C.; Shen, G. Z.; Chen, H.; Ha, Y. G.; Wu, C.; Sukcharoenchoke, S.; Fu, Y.; Liu, J.; Facchetti, A.; Marks, T. J.; *et al.* High-Performance Single-Crystalline Arsenic-Doped Indium Oxide Nanowires for Transparent Thin Film Transistors and Active Matrix Organic Light-Emitting Diode Displays. *ACS Nano* **2009**, *3*, 3383–3390.